

# resonator-assisted single-photon frequency conversion in a conventional waveguide with a giant V-type atom

Ge Sun,<sup>1, 2</sup> Hongzheng Wu,<sup>1, 2</sup> Jing Lu,<sup>1, 2</sup> and Lan Zhou<sup>1, 2, \*</sup>

<sup>1</sup>*Key Laboratory of Low-Dimension Quantum Structures and Quantum Control of Ministry of Education, Key Laboratory for Matter Microstructure and Function of Hunan Province, Synergetic Innovation Center for Quantum Effects and Applications, Xiangjiang-Laboratory and Department of Physics, Hunan Normal University, Changsha 410081, China*

<sup>2</sup>*Institute of Interdisciplinary Studies, Hunan Normal University, Changsha, 410081, China*

We propose a scheme to achieve efficient frequency conversion for a single photon propagating in a 1D conventional waveguide by exploiting the quantum interference induced by the scale of a V-type giant atom (GA) characterized by the distance between the two coupling points as well as single-photon transition pathways originated from the coupling between the GA and the resonator. The presence of photons in the resonator triggers the frequency conversion of photons. The scattering spectra and the conversion contrast are studied in both the Markovian and the non-Markovian regimes. The disappearance of frequency conversion is rooted in the complete suppression of the emission from the excited state to either of lower states in the  $n+1$  subspace where  $n$  is the photon number of the resonator, and the non-Markovicity-induced nonreciprocity is found under specific conditions. Altering the photon number  $n$  induces the non-reciprocal transmission of single photons in the waveguide, hence, enhance the conversion probability.

## I. INTRODUCTION

Quantum networks[1] connect individual quantum systems via quantum channels. Propagating photons are ideal flying qubits in quantum channels for carry quantum information over long distances with almost negligible decoherence. Precise control over single photons is required by creating large-scale, distributed quantum networks for technologies such as computing, communication, sensing [2], and metrology [3]. The lack of a direct interaction between photons at the single-photon level in vacuum makes it necessary to rely on coupling with quantum emitters (QEs). The coupling of QEs to propagating fields is desirable in quantum network. However, the single-photon-single-QE coupling is too weak in free space, the coupling can be substantially increased by placing the QEs in waveguide structures [4], which confine photons to a one-dimensional (1D) environment. This kind of setup is termed as waveguide-QED systems [5].

To incorporate all the benefits needed, quantum systems in quantum networks operate at dissimilar frequencies in order to perform each task at its optimal frequency. It is desired to alter single photons from one frequency to another frequency in order to implement hybrid quantum information processing at different energy scales. Based on waveguide-QED systems, frequency converter have been proposed for single photons by a point-like three-level QE locally coupled to a Sagnac interferometer [6, 7], a coupled-resonator waveguide [8], a semi-infinite 1D transmission line [9]. With the great technological progress to the chip scale, the waveguide-

QED system has been generalized to studies of a QE nonlocally coupled to photons in the waveguide [10–23]. The quantum emitter with dimension comparable to or larger than the wavelength of its emitted photon is called giant atom (GA). A GA-waveguide system can be realized by superconducting artificial QEs coupled to surface acoustic waves [24–26] or microwaves through multiple coupling points through suitably meandering the transmission line with wavelength-scale distance [27]. Frequency conversions for a 1D waveguide with a GA have been proposed in Ref. [28, 29]. By employing the Markovian approximation, the conversion efficiency is at most one-half in a conventional waveguide in Ref [28]. Via the chiral GA-waveguide couplings, the single-photon conversion efficiency is enhanced to unity in Ref. [29]. In this paper, we propose single-photon frequency conversion for a single photon propagating in a 1D *conventional* waveguide scattered by a V-type GA coupled to a single-mode resonator. For a conventional waveguide, the couplings strengths of the GA to the right-going and left-going field modes are equal. The frequency of the photon propagating in 1D waveguide is possible to be converted up or down as long as photons are present in the resonator, and the frequency shift is controlled by the number of photons in the resonator. By utilizing a real-space scattering method [30, 31], the single-photon scattering spectra are obtained for a single photon incidence from the waveguide and the number of excitations in the GA and the resonator. We analyze the influences of phase delay between coupling points, the phase difference between two GA-waveguide couplings and the number of photons in the resonator on the scattering spectra in both the Markovian and the non-Markovian regimes. It is found that the frequency conversion vanishes when the emission from the excited state to either of lower states is complete suppressed in the  $n+1$  subspace where  $n$  is

\* Corresponding author; zhoulan@hunnu.edu.cn

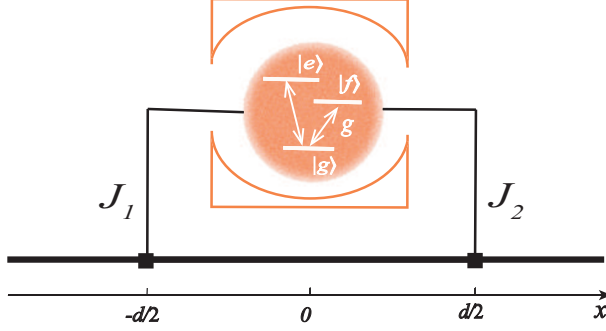


FIG. 1. Sketch of a V-type three-level atom coupled to a one-dimensional waveguide. The transition  $|g\rangle \leftrightarrow |e\rangle$  is coupled to the waveguide at positions  $x = \pm d/2$ , while the transition  $|g\rangle \leftrightarrow |f\rangle$  is coupled to a single-mode cavity.

the photon number of the resonator. By adjusting the number of photons in the resonator, the non-reciprocal transmission of single photons is present, and the conversion probability for single photons can be achieved with unity efficiency.

## II. THE SYSTEM OF A GA COUPLED TO A 1D WAVEGUIDE AND A RESONATOR

We consider three energy levels  $|g\rangle, |f\rangle, |e\rangle$  of a single GA forming a V configuration as illustrated in Fig.1. The ground state  $|g\rangle$  is separated to state  $|e\rangle$  ( $|f\rangle$ ) in frequency by  $\omega_e$  ( $\omega_f$ ), and it can either transit to state  $|f\rangle$  by a single-mode resonator of frequency  $\omega_c$  with  $\hat{b}$  represented its annihilating operator, or transit to state  $|e\rangle$  via absorbing a propagating photon in the waveguide at positions  $x_1 = -d/2$ ,  $x_2 = d/2$ . Denoting  $\hat{a}_L(x)$  and  $\hat{a}_R(x)$  as the field operators of annihilating the right- and left-traveling photons at position  $x$  in waveguide, the full Hamiltonian of the system reads

$$\begin{aligned} \hat{H} = & \hat{H}_0 + \left( g\hat{b}^\dagger |g\rangle\langle f| + h.c. \right) \\ & + \sum_{j=1}^2 \int dk J_j \delta(x - x_j) e^{(-1)^j i k_0 \frac{d}{2}} \hat{a}_L^\dagger(x) |g\rangle\langle e| + h.c. \\ & + \sum_{j=1}^2 \int dk J_j \delta(x - x_j) e^{-(1)^j i k_0 \frac{d}{2}} \hat{a}_R^\dagger(x) |g\rangle\langle e| + h.c. \end{aligned} \quad (1)$$

with the free Hamiltonian

$$\begin{aligned} H_0 = & \omega_f |f\rangle\langle f| + \omega_e |e\rangle\langle e| + \omega_c \hat{b}^\dagger \hat{b} \\ & + \int_{-\infty}^{\infty} dx \hat{a}_R^\dagger(x) \left( \omega_0 - iv \frac{\partial}{\partial x} \right) \hat{a}_R(x) \\ & + \int_{-\infty}^{\infty} dx \hat{a}_L^\dagger(x) \left( \omega_0 + iv \frac{\partial}{\partial x} \right) \hat{a}_L(x). \end{aligned}$$

where coefficient  $g$  and  $J_j = |J_j| e^{i\varphi_j}$  define the coupling strengths of the GA to the resonator and the waveguide respectively,  $\omega_0$  is the central frequency around which a linear dispersion relation under consideration is given by  $\omega(k) = \omega_0 + v(k - k_0)$ ,  $v$  is the group velocity in the vicinity of  $\omega_0$ . No direct coupling is assumed between the resonator and waveguide.

We assume that the GA is initially in its ground state, the resonator contains  $n$  b-mode photons. A photon coming from either side of the waveguide is scattered by the GA-resonator interaction. When  $n = 0$ , the GA absorbs the input photon and transit from  $|g\rangle$  to its excited state  $|e\rangle$ , then back to its ground state by re-emitting the photon. In this case, the system becomes a two-level GA interacting with the waveguide since state  $|f\rangle$  does not participate in the dynamic process, and it is impossible for the frequency of the photon to be converted. As long as  $n \neq 0$ , the transition  $|e\rangle \leftrightarrow |f\rangle$  is allowed, the quantum interference between different transitions of the GA leads to behaviors different from  $n = 0$ . The exchange of excitations between the GA and the resonator mode raises (lowers) the state  $|g\rangle$  ( $|f\rangle$ ) of the GA to the state  $|f\rangle$  ( $|g\rangle$ ) and lower (raise) the number of photons in the resonator from  $n$  ( $n - 1$ ) to  $n - 1$  ( $n$ ). The GA-resonator coupling changes the bare states of the GA and resonator to the following dressed states

$$|n_+\rangle = \sin \frac{\theta_n}{2} |gn\rangle + \cos \frac{\theta_n}{2} |fn - 1\rangle \quad (2a)$$

$$|n_-\rangle = -\cos \frac{\theta_n}{2} |gn\rangle + \sin \frac{\theta_n}{2} |fn - 1\rangle \quad (2b)$$

with the corresponding eigenenergies  $\lambda_{n\pm} = n\omega_c + \nu_\pm^n$  and  $\tan \theta_n = 2\sqrt{n}g/\omega_{fc}$ , where  $\omega_{fc} = \omega_f - \omega_c$  and

$$\nu_\pm^n = \frac{\omega_{fc} \pm \sqrt{\omega_{fc}^2 + 4n|g|^2}}{2}. \quad (3)$$

When the GA is excited by an incoming photon in the waveguide exactly on resonance with the  $|e\rangle \leftrightarrow |n_-\rangle$  transition, it will spontaneously decay to either  $|n_-\rangle$  or  $|n_+\rangle$  and emit a photon, a frequency down-conversion is achieved when the GA decays to state  $|n_+\rangle$ . Alternatively, frequency up-conversion can be realized by initializing the GA in state  $|n_+\rangle$  and an incoming photon on resonance with the  $|e\rangle \leftrightarrow |n_+\rangle$  transition. Thence, the presence of photons in the resonator triggers frequency conversion.

Since the total number of excitations in this system is conserved, states  $\hat{a}_R^\dagger(x)|n_{\pm 0}\rangle$ ,  $\hat{a}_L^\dagger(x)|n_{\pm 0}\rangle$ ,  $|en0\rangle$  form basis of the subspace with  $n+1$  excitations, and they can expand the eigenstate in this subspace as

$$|\psi_{n+1}\rangle = \sum_{P,\alpha} \int_{-\infty}^{\infty} dx P_\alpha^n(x) \hat{a}_P^\dagger(x) |n_{\alpha 0}\rangle + u_{ne} |en0\rangle \quad (4)$$

with  $P = R, L$  and  $\alpha = \pm$ . Here,  $R_\alpha^n(x)$  ( $L_\alpha^n(x)$ ) is the single-photon wave function of a right-moving (left-moving) photon in the waveguide at position  $x$  and the

GA-resonator in state  $|n_\alpha\rangle$ ,  $u_{ne}$  is the probability amplitude for all modes of the waveguide in vacuum states, the resonator mode in the number state  $n$ , and the 3GA in its excited state. The Schrödinger eigen-equation yields

the equations for the field amplitudes

$$ER_+^n(x) = \left(\omega_+^n - iv\frac{\partial}{\partial x}\right)R_+^n(x) + V_{n+}^R u_{ne}, \quad (5a)$$

$$EL_+^n(x) = \left(\omega_+^n + iv\frac{\partial}{\partial x}\right)L_+^n(x) + V_{n+}^L u_{ne}, \quad (5b)$$

$$ER_-^n(x) = \left(\omega_-^n - iv\frac{\partial}{\partial x}\right)R_-^n(x) - V_{n-}^R u_{ne}, \quad (5c)$$

$$EL_-^n(x) = \left(\omega_-^n + iv\frac{\partial}{\partial x}\right)L_-^n(x) - V_{n-}^L u_{ne}, \quad (5d)$$

and the amplitude for the excited state of the GA

---


$$\begin{aligned} Eu_{ne} = & (\omega_e + n\omega_c)u_{ne} \\ & + J_{1+}^* \int dx \delta\left(x + \frac{d}{2}\right) \left[ e^{-ik_0 \frac{d}{2}} R_+^n(x) + e^{ik_0 \frac{d}{2}} L_+^n(x) \right] - J_{1-}^* \int dx \delta\left(x + \frac{d}{2}\right) \left[ e^{-ik_0 \frac{d}{2}} R_-^n(x) + e^{ik_0 \frac{d}{2}} L_-^n(x) \right] \\ & + J_{2+}^* \int dx \delta\left(x - \frac{d}{2}\right) \left[ e^{ik_0 \frac{d}{2}} R_+^n(x) + e^{-ik_0 \frac{d}{2}} L_+^n(x) \right] - J_{2-}^* \int dx \delta\left(x - \frac{d}{2}\right) \left[ e^{ik_0 \frac{d}{2}} R_-^n(x) + e^{-ik_0 \frac{d}{2}} L_-^n(x) \right], \end{aligned} \quad (6)$$


---

where we have defined

$$\omega_\pm^n = \omega_0 + n\omega_c + \nu_\pm^n, \quad (7a)$$

$$J_{i+}^n = J_i \sin \frac{\theta_n}{2}, J_{i-}^n = J_i \cos \frac{\theta_n}{2}, \quad (7b)$$

$$V_{n\pm}^R = J_{1\pm}^n e^{ik_0 \frac{d}{2}} \delta\left(x + \frac{d}{2}\right) + J_{2\pm}^n e^{-ik_0 \frac{d}{2}} \delta\left(x - \frac{d}{2}\right), \quad (7c)$$

$$V_{n\pm}^L = J_{1\pm}^n e^{-ik_0 \frac{d}{2}} \delta\left(x + \frac{d}{2}\right) + J_{2\pm}^n e^{ik_0 \frac{d}{2}} \delta\left(x - \frac{d}{2}\right). \quad (7d)$$

The wave function for the photon incident from the left-side takes the following form:

$$\begin{aligned} R_-^n(x) = & \left[ \Theta\left(-x - \frac{d}{2}\right) + t_-^n \Theta\left(x - \frac{d}{2}\right) \right] e^{ik_n x} \\ & + A_-^n \Theta\left(x + \frac{d}{2}\right) \Theta\left(\frac{d}{2} - x\right) e^{ik_n x}, \end{aligned} \quad (8a)$$

$$L_-^n(x) = \left[ r_-^n \Theta\left(-x - \frac{d}{2}\right) + B_-^n \Theta\left(\frac{d}{2} - |x|\right) \right] e^{-ik_n x}, \quad (8b)$$

$$R_+^n(x) = \left[ M^n \Theta\left(\frac{d}{2} - |x|\right) + t_+^n \Theta\left(x - \frac{d}{2}\right) \right] e^{iq_n x}, \quad (8c)$$

$$L_+^n(x) = \left[ r_+^n \Theta\left(-x - \frac{d}{2}\right) + N^n \Theta\left(\frac{d}{2} - |x|\right) \right] e^{-iq_n x}, \quad (8d)$$

where  $\Theta(x)$  is the Heaviside step function,  $t_-^n$  and  $r_-^n$  are the single-photon transmission and reflection amplitudes with wave vectors  $k_n = (E - \omega_-^n)/v$  and  $-k_n$  when the GA is in state  $|n_-\rangle$ ,  $t_+^n$  and  $r_+^n$  are the single-photon conversion amplitudes with wave vectors  $q_n = (E - \omega_+^n)/v$  and  $-q_n$  when the GA is in state  $|n_+\rangle$ . So the continuum of the waveguide can be divided as a  $n_-$ -channel and a  $n_+$ -channel according to the GA in state  $|n_-\rangle$  or  $|n_+\rangle$ . The transmittance  $T_-^n = |t_-^n|^2$  and the reflectance  $R_-^n = |r_-^n|^2$  describe the elastic scattering process which preserves the original frequency of single photons. The conversion probability  $T_c^n = |r_+^n|^2 + |t_+^n|^2$  describes the inelastic scattering process which changes the frequency of propagating photons by the amount  $|\lambda_{n+} - \lambda_{n-}|$ . The scatter spectra significantly depend on the spontaneous damping rates  $\Gamma_\pm^n$  from the excited state  $|e\rangle$  to state  $|n_\pm\rangle$  due to the coupling of the GA to the vacuum field, and the nonlocal damping rates  $\gamma_\pm^n$  from the coupling of the GA through the vacuum field at different points

$$\Gamma_+^n = \Gamma \sin^2 \frac{\theta_n}{2}, \Gamma_-^n = \Gamma \cos^2 \frac{\theta_n}{2} \quad (9a)$$

$$\gamma_+^n = \frac{2|J_1 J_2|}{v} \sin^2 \frac{\theta_n}{2} \cos \varphi_J \quad (9b)$$

$$\gamma_-^n = \frac{2|J_1 J_2|}{v} \cos^2 \frac{\theta_n}{2} \cos \varphi_J \quad (9c)$$

with  $\Gamma = (|J_1|^2 + |J_2|^2)/v$  and  $\varphi_J = \varphi_2 - \varphi_1$ . The scattering amplitudes for a left-incident photon in the  $n_-$ -channel read

$$t_-^n = \frac{\Delta_k^n - 2\frac{J_{1-}^n J_{2-}^n}{v} \sin(\Delta_k^n \tau + \phi_-^n) + i\Gamma_+^n + i\gamma_+^n e^{i\Delta_k^n \tau} e^{i\phi_+^n}}{\Delta_k^n + i(\Gamma_+^n + \gamma_+^n e^{i\Delta_k^n \tau} e^{i\phi_+^n}) + i(\Gamma_-^n + \gamma_-^n e^{i\Delta_k^n \tau} e^{i\phi_-^n})}, \quad (10a)$$

$$r_-^n = -\frac{i\gamma_- + \frac{i}{v} \left[ |J_{1-}^n|^2 e^{-i(\Delta_k^n \tau + \phi_-^n)} + |J_{2-}^n|^2 e^{i(\Delta_k^n \tau + \phi_-^n)} \right]}{\Delta_k^n + i(\Gamma_+^n + \gamma_+^n e^{i\Delta_k^n \tau} e^{i\phi_+^n}) + i(\Gamma_-^n + \gamma_-^n e^{i\Delta_k^n \tau} e^{i\phi_-^n})}, \quad (10b)$$

$$r_+^n = \frac{\frac{ie^{-i\phi_n}}{v} [J_{1+}^n e^{-i(\Delta_k^n \tau + \phi_+^n)} + J_{2+}^n] \left[ J_{1-}^{n*} + J_{2-}^{n*} e^{i(\Delta_k^n \tau + \phi_-^n)} \right]}{\Delta_k^n + i(\Gamma_+^n + \gamma_+^n e^{i\Delta_k^n \tau} e^{i\phi_+^n}) + i(\Gamma_-^n + \gamma_-^n e^{i\Delta_k^n \tau} e^{i\phi_-^n})}, \quad (10c)$$

$$t_+^n = \frac{\frac{ie^{-i\phi_n}}{v} [J_{1+}^n + J_{2+}^n e^{-i(\Delta_k^n \tau + \phi_+^n)}] \left[ J_{1-}^{n*} + J_{2-}^{n*} e^{i(\Delta_k^n \tau + \phi_-^n)} \right]}{\Delta_k^n + i(\Gamma_+^n + \gamma_+^n e^{i\Delta_k^n \tau} e^{i\phi_+^n}) + i(\Gamma_-^n + \gamma_-^n e^{i\Delta_k^n \tau} e^{i\phi_-^n})}, \quad (10d)$$

where  $\Delta_k^n = \omega_0 + vk_n - (\omega_e - \nu_-^n)$  is the detuning between the input photon and the  $|e\rangle \leftrightarrow |n-\rangle$  transition,

the accumulated phases

$$\phi_{\pm}^n = (\omega_e - v_{n\pm})\tau, \phi_n = (v_{n+} - v_{n-})\tau, \quad (11)$$

and  $\tau = d/v$  is the delay time that photons travel along the distance between two connection points.

For the photon incident from the far right of GA initial in the  $n_-$ -channel, scattering amplitudes read

$$\tilde{t}_-^n = \frac{\Delta_k^n - 2\frac{J_{1-}^n J_{2-}^n}{v} \sin(\Delta_k^n \tau + \phi_-^n) + i\Gamma_+^n + i\gamma_+^n e^{i\Delta_k^n \tau} e^{i\phi_+^n}}{\Delta_k^n + i(\Gamma_+^n + \gamma_+^n e^{i\Delta_k^n \tau} e^{i\phi_+^n}) + i(\Gamma_-^n + \gamma_-^n e^{i\Delta_k^n \tau} e^{i\phi_-^n})}, \quad (12a)$$

$$\tilde{r}_-^n = -\frac{i\gamma_- + i\frac{|J_{1-}^n|^2}{v} e^{i(\Delta_k^n \tau + \phi_-^n)} + i\frac{|J_{2-}^n|^2}{v} e^{-i(\Delta_k^n \tau + \phi_-^n)}}{\Delta_k^n + i(\Gamma_+^n + \gamma_+^n e^{i\Delta_k^n \tau} e^{i\phi_+^n}) + i(\Gamma_-^n + \gamma_-^n e^{i\Delta_k^n \tau} e^{i\phi_-^n})}, \quad (12b)$$

$$\tilde{r}_+^n = \frac{\frac{ie^{i\phi_n}}{v} (J_{1+}^n e^{i\Delta_k^n \tau} e^{i\phi_+^n} + J_{2+}^n) (J_{1-}^{n*} + J_{2-}^{n*} e^{-i\Delta_k^n \tau} e^{-i\phi_-^n})}{\Delta_k^n + i(\Gamma_+^n + \gamma_+^n e^{i\Delta_k^n \tau} e^{i\phi_+^n}) + i(\Gamma_-^n + \gamma_-^n e^{i\Delta_k^n \tau} e^{i\phi_-^n})}, \quad (12c)$$

$$\tilde{t}_+^n = \frac{\frac{ie^{i\phi_n}}{v} (J_{1+}^n + J_{2+}^n e^{i\Delta_k^n \tau} e^{i\phi_+^n}) (J_{1-}^{n*} + J_{2-}^{n*} e^{-i\Delta_k^n \tau} e^{-i\phi_-^n})}{\Delta_k^n + i(\Gamma_+^n + \gamma_+^n e^{i\Delta_k^n \tau} e^{i\phi_+^n}) + i(\Gamma_-^n + \gamma_-^n e^{i\Delta_k^n \tau} e^{i\phi_-^n})}. \quad (12d)$$

Similarly, the transmittance  $\tilde{T}_-^n = |\tilde{t}_-^n|^2$  and the reflectance  $\tilde{R}_-^n = |\tilde{r}_-^n|^2$  describe the elastic scattering process in the incident channel, which can be called  $n_-$ -channel since the GA is initially in  $|n-\rangle$ . For the GA ending in state  $|n_+\rangle$ , the photon is scattered inelastically and propagates in the  $n_+$ -channel with the conversion probability  $\tilde{T}_c^n = |\tilde{r}_+^n|^2 + |\tilde{t}_+^n|^2$ . We will only study the transport properties for single photons incidence from the  $n_-$ -channel since the discussion is similar for photons incidence from the  $n_+$ -channel. The interaction with the vacuum fluctuations of the waveguide generates the Lamb shift

$$\delta_k^n = \gamma_+^n \sin(\Delta_k^n \tau + \phi_+^n) + \gamma_-^n \sin(\Delta_k^n \tau + \phi_-^n) \quad (13)$$

and the interference effects of reemitted photons from different coupling points modified decay rates into the

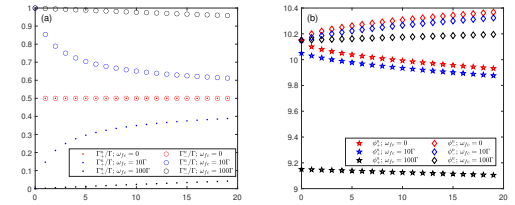


FIG. 2. (a) The spontaneous damping rates  $\Gamma_{\pm}^n$  and (b) the accumulated phases  $\phi_{\pm}^n$  versus photon number  $n$  with  $g = 5\Gamma, \omega_e = 1015\Gamma$ , and  $\Gamma\tau = 0.01$ .

effective decay rate

$$\tilde{\Gamma}_k^n = \sum_{\alpha=\pm} [\Gamma_{\alpha}^n + \gamma_{\alpha}^n \cos(\Delta_k^n \tau + \phi_{\alpha}^n)], \quad (14)$$

which change periodically with  $\Delta_k^n$ . It can be found

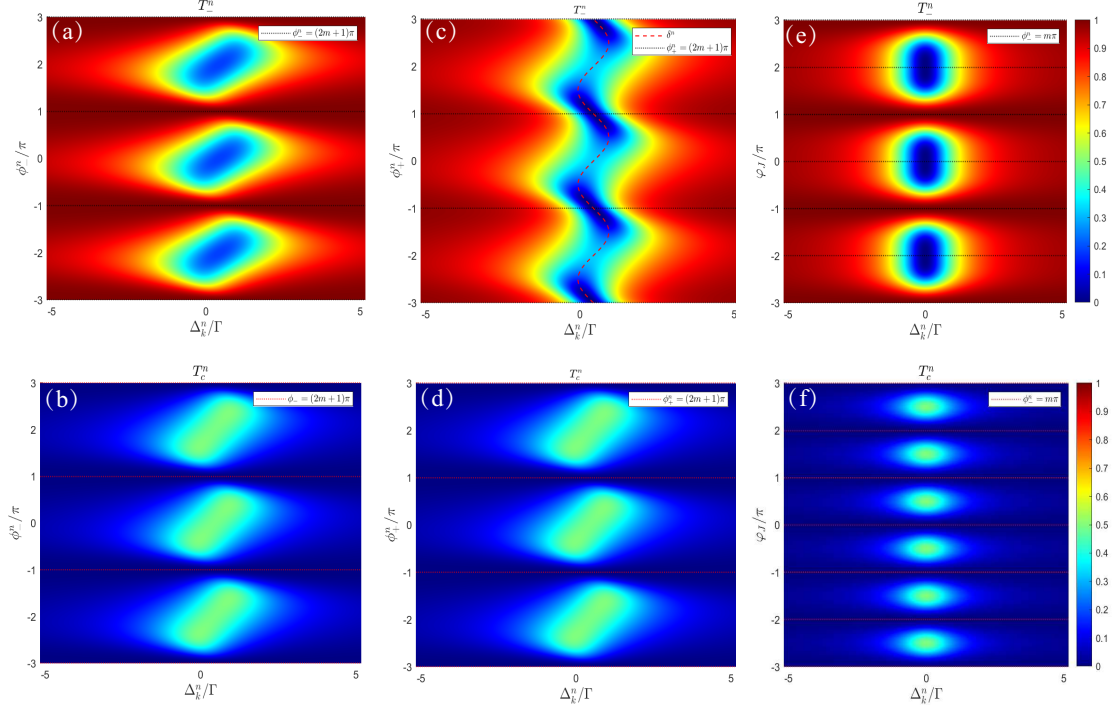


FIG. 3. (a,c,e) The transmittance  $T_-^n$  and (b,d,f) the conversion probability  $T_c^n$  verse the scaled detuning  $\Delta_k^n$  and the scaled phase (a,b)  $\phi_-^n/\pi$ , (c,d)  $\phi_+^n/\pi$ , (e,f)  $\varphi_J/\pi$  when  $n = 1$ ,  $|J_1| = |J_2|$  and  $\omega_{fc} = 0$ . Other parameters are setting as follow: (a,b)  $\varphi_J = 0$  and  $\phi_+^n = \pi/3$ ; (c,d)  $\varphi_J = 0$  and  $\phi_-^n = \pi/3$ ; (e,f)  $\phi_-^n = 0$  and  $\phi_+^n = \pi$ .

from Eqs.(10) and (12) that the reflectance  $R_-^n = \tilde{R}_-^n$ , and the system presents reciprocity in transmission and conversion upon reversing the propagation of an incident photon when  $\varphi_J = n\pi$ . To quantitatively describe the nonreciprocity, we define the transmission contrast  $I_1^n = T_-^n - \tilde{T}_-^n$  and the conversion contrast  $I_2^n = T_c^n - \tilde{T}_c^n$ . The energy conservation in the system indicates  $I_1^n = -I_2^n$ . The reciprocal scattering corresponds to  $I_1^n = I_2^n = 0$ . As the scattering coefficients can not be smaller than zero,  $|I_1^n| = |I_2^n| = 1$  depicts the optimal nonreciprocal scattering corresponding to the unity efficiency of the frequency conversion.

### III. THE SCATTERING SPECTRA AND THE CONVERSION CONTRAST

The GA-resonator system forms an effective two-legged GA with multiple levels in the presence of photons in the resonator. In the  $(n+1)$ -excitation subspace with only one photon in the waveguide, the GA-resonator system form an effective  $\Lambda$ -type GA, however, the couplings of the GA to the left-going and right-going modes are equal at each connection points, which can be explicitly found in Hamiltonian (1). The scattering spectra are determined by the following parameters: the characteristic frequencies  $\omega_e - \lambda_{n\pm}$ , the delay time  $\tau$ , the decay rate  $\Gamma$ , and the number  $n$  of photons in the resonator. Now, we will set  $|J_j| = J$  since the system reduces to a two-

level GA interaction with a 1D waveguide and photonic bound states in continuum (BIC)[32–38] can be found for an injected photon when  $n = 0$ , then  $\gamma_{\pm}^n = \Gamma_{\pm}^n \cos \varphi_L$ . In Fig. 2, we plot  $\Gamma_{\pm}^n$  and  $\phi_{\pm}^n$  as a function of the photon number  $n$  when  $\omega_{fc} = 0$ ,  $\omega_{fc} \sim g$  and  $\omega_{fc} \gg g$ , respectively. It can be observed from Fig.2a that  $\Gamma_{\pm}^n = \Gamma/2$  for resonance  $\omega_{fc} = 0$  (see the red dots and circles),  $\Gamma_-^n \approx \Gamma$  and  $\Gamma_+^n \approx 0$  for lager detuning  $\omega_{fc} \gg g$  (see the black dots and circles), and  $\Gamma_-^n$  decreases but  $\Gamma_+^n$  increases as  $n$  increases for  $\omega_{fc} \sim g$  (see the blue dots and circles). Fig. 2b shows that  $\phi_{\pm}^n$  hardly varies with  $n$  at lager detuning  $\omega_{fc} \gg g$  (see the black stars and diamonds), they all changes with  $n$  at the other two cases. In the following discussion, we will assume that the resonator is on resonance with the  $|g\rangle \leftrightarrow |f\rangle$  transition of the GA, the spontaneous damping rates  $\Gamma_{\pm}^n$  and the nonlocal damping rates  $\gamma_{\pm}^n$  can be rewritten as  $\Gamma/2$  and  $\gamma_{\pm}^n = (\Gamma/2) \cos \varphi_J$  as  $\theta_n = \pi/2$  in Eq.(2) is fixed, however,  $\phi_{\pm}^n$  takes different values for different  $n$ . In a GA-waveguide system,  $\tau^{-1}, \Gamma < \omega_e - \lambda_{n\pm}$  is usually satisfied. Thus, the spectra of single photons are decided by the propagation time  $\tau$  and the lifetime  $\Gamma^{-1}$ .

#### A. Markovian regime

In the Markovian regime, the delay time  $\tau$  due to photon travelling between coupling points is much smaller than the lifetime  $\Gamma^{-1}$ . the factors  $\exp(\pm i \Delta_k^n \tau) \approx 1$ , Then

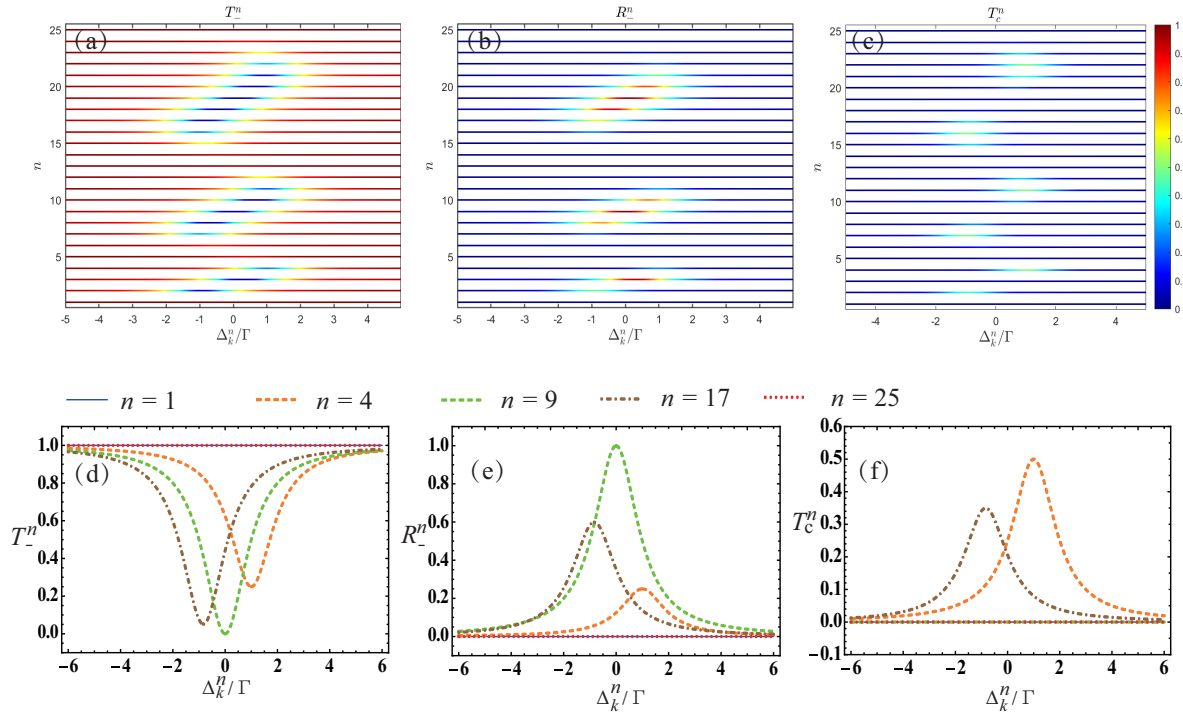


FIG. 4. The transmittance (a)  $T_-^n$ , reflectance (b)  $R_-^n$ , and conversion probability (c)  $T_c^n$  versus photon number  $n$  and the scaled detuning  $\Delta_k^n/\Gamma$  when  $|J_1| = |J_2|$ ,  $\omega_{fc} = 0$ ,  $\omega_e/\Gamma = 1015$ ,  $g/\Gamma = 15$ ,  $\varphi_J = 0$ ,  $\tau\Gamma = 0.1\pi$ . (d-f) The profile of the scattering spectra at  $n = 1, 4, 9, 17, 25$ .

the corresponding scattering amplitudes read

$$t_-^n = \frac{\Delta_k^n - 2 \frac{J_{1-}^{n*} J_{2-}^n}{v} \sin \phi_-^n + i (\Gamma_+^n + \gamma_+^n e^{i\phi_+^n})}{\Delta_k^n + i (\Gamma_+^n + \gamma_+^n e^{i\phi_+^n}) + i (\Gamma_-^n + \gamma_-^n e^{i\phi_-^n})} \quad (15a)$$

$$r_-^n = -\frac{i\gamma_- + \frac{i}{v} (|J_{1-}^n|^2 e^{-i\phi_-^n} + |J_{2-}^n|^2 e^{i\phi_-^n})}{\Delta_k^n + i (\Gamma_+^n + \gamma_+^n e^{i\phi_+^n}) + i (\Gamma_-^n + \gamma_-^n e^{i\phi_-^n})} \quad (15b)$$

$$r_+^n = \frac{\frac{ie^{-i\phi_+}}{v} (J_{1+}^n e^{-i\phi_{n+}} + J_{2+}^n) (J_{1-}^{n*} + J_{2-}^{n*} e^{i\phi_-^n})}{\Delta_k^n + i (\Gamma_+^n + \gamma_+^n e^{i\phi_+^n}) + i (\Gamma_-^n + \gamma_-^n e^{i\phi_-^n})} \quad (15c)$$

$$t_+^n = \frac{\frac{ie^{-i\phi_+}}{v} (J_{1+}^n + J_{2+}^n e^{-i\phi_+^n}) (J_{1-}^{n*} + J_{2-}^{n*} e^{i\phi_-^n})}{\Delta_k^n + i (\Gamma_+^n + \gamma_+^n e^{i\phi_+^n}) + i (\Gamma_-^n + \gamma_-^n e^{i\phi_-^n})} \quad (15d)$$

for light injected from the left side of the GA and

$$\tilde{t}_-^n = \frac{\Delta_k^n - 2 \frac{J_{1-}^{n*} J_{2-}^n}{v} \sin \phi_-^n + i \Gamma_+^n + i \gamma_+^n e^{i\phi_+^n}}{\Delta_k^n + i (\Gamma_+^n + \gamma_+^n e^{i\phi_+^n}) + i (\Gamma_-^n + \gamma_-^n e^{i\phi_-^n})} \quad (16a)$$

$$\tilde{r}_-^n = -\frac{i\gamma_- + \frac{i}{v} (|J_{1-}^n|^2 e^{i\phi_-^n} + |J_{2-}^n|^2 e^{-i\phi_-^n})}{\Delta_k^n + i (\Gamma_+^n + \gamma_+^n e^{i\phi_+^n}) + i (\Gamma_-^n + \gamma_-^n e^{i\phi_-^n})} \quad (16b)$$

$$\tilde{r}_+^n = \frac{\frac{i}{v} e^{i\phi_+} (J_{1+}^n e^{i\phi_+^n} + J_{2+}^n) (J_{1-}^{n*} + J_{2-}^{n*} e^{-i\phi_-^n})}{\Delta_k^n + i (\Gamma_+^n + \gamma_+^n e^{i\phi_+^n}) + i (\Gamma_-^n + \gamma_-^n e^{i\phi_-^n})} \quad (16c)$$

$$\tilde{t}_+^n = \frac{\frac{i}{v} e^{i\phi_+} (J_{1+}^n + J_{2+}^n e^{i\phi_+^n}) (J_{1-}^{n*} + J_{2-}^{n*} e^{-i\phi_-^n})}{\Delta_k^n + i (\Gamma_+^n + \gamma_+^n e^{i\phi_+^n}) + i (\Gamma_-^n + \gamma_-^n e^{i\phi_-^n})} \quad (16d)$$

for light injected from the right side of the GA. The Lamb shift  $\delta^n = \gamma_+^n \sin \phi_+^n + \gamma_-^n \sin \phi_-^n$  and the effective decay rate  $\tilde{\Gamma}^n = \sum_{\alpha=\pm} (\Gamma_\alpha^n + \gamma_\alpha^n \cos \phi_\alpha^n)$  are independent on the incident energy of the photon. In Fig. 3, we have plotted the transmittance and the conversion probability as a function of  $\Delta_k^n$  and a phase when  $n = 1$ . All scattering coefficients change periodically with the phase. The transmission spectra  $T_-^n = \tilde{T}_-^n$  possess an anti-Lorentzian lineshape centered at  $\delta^n$  with a nonzero/zero minimum in Fig. 3(a)/(c), the conversion probability  $T_c^n = \tilde{T}_c^n$  have the standard Lorentzian lineshapes centered at  $\delta^n$  with a maximum 0.5. The width of the transmission spectra first increase and then decrease as  $\phi_\pm^n$  changes from  $-\pi$  to  $\pi$  and reaches its maximum at  $\phi_\pm^n = 0$ , so does the width of the conversion probability. One can also observed a frequency-independent perfect transmission at  $\varphi_J = 2m\pi$  and  $\phi_-^n = (2m+1)\pi$  in Fig. 3(a) and a transmittance dropping to zero at  $\varphi_J = 2m\pi$  and  $\phi_+^n = (2m+1)\pi$  in Fig. 3(c), however, the frequency conversion is completely suppressed at either  $\phi_-^n = (2m+1)\pi$  or  $\phi_+^n = (2m+1)\pi$  (see the red dotted line in 3b, 3d), which indicates that reflectance  $R_-^n = \tilde{R}_-^n = 0$  at  $\varphi_J = 2m\pi$  and  $\phi_-^n = (2m+1)\pi$ , and  $R_-^n = \tilde{R}_-^n = 1$  at  $\delta^n$  when  $\varphi_J = 2m\pi$  and  $\phi_+^n = (2m+1)\pi$  since the probability for the photon is conserved. The frequency-independent perfect transmission can also be observed in Fig. 3(e) when  $\varphi_J = (2m+1)\pi$

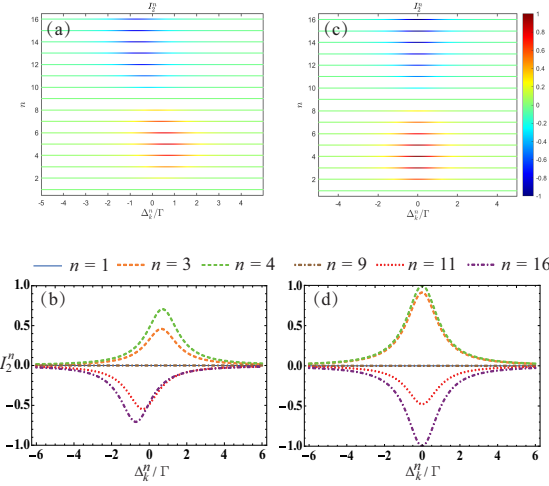


FIG. 5. The conversion contrast  $I_2^n$  versus photon number  $n$  and the scaled detuning  $\Delta_k^n/\Gamma$  when  $|J_1| = |J_2|$ ,  $\omega_{fc} = 0$ ,  $\omega_e/\Gamma = 1015$ ,  $g/\Gamma = 5$ ,  $\tau\Gamma = 0.1\pi$ . (a)  $\varphi_J = 0.25\pi$ , (c)  $\varphi_J = 0.5\pi$ . (b,d) The profile of the conversion contrast at  $n = 1, 3, 4, 9, 11, 16$ .

and  $\phi_-^n = 2m\pi$ . Substituting the parameters for the frequency conversion vanishing into Eq.(15) and (16), we found that the emission of the GA to the continuum of the  $n_-$ -channel ( $n_+$ -channel) is completely suppressed at  $\varphi_J = m\pi$  and  $\phi_+^n = (m + 1)\pi$  for arbitrary  $\phi_+^n$  ( $\varphi_J = m\pi$  and  $\phi_+^n = (m + 1)\pi$  for arbitrary  $\phi_-^n$ ), which leads to the formation of GA-photon bound state[39–41] in the  $n_-$ -channel ( $n_+$ -channel). The GA-photon bound state gives rise to the BIC. Consequently, the number of zeros in the frequency conversion is greater in Fig. 3(f) than in Fig. 3(b,d). We note that the optimal  $T_c^n$  is at most, one-half when  $\varphi_J = (m + 1/2)\pi$  in Fig. 3(f),  $T_c^n \leq 1/2$  can also be observed in Fig. 3(b,d) when  $\varphi_J = m\pi$ , this is because photon scattering coefficients with either  $\varphi_J = m\pi$  or  $\phi_-^n = m\pi$  are symmetric for the forward and backward propagating photons, which can be found from Eq. (15a) and (16a).

To investigate the influence of the number  $n$  of photons in the resonator on the scattering spectra, we plot the transmittance, the reflectance and the conversion probability versus the detuning and the photon number  $n$  in the resonator for  $\varphi_J = 0$  in Fig.4 with other parameters satisfying a frequency-independent perfect transmission in the  $1 + 1$  subspace. The scattering spectra are also periodic functions of  $n$ . As  $n$  increases, the transmittance gradually decreases to zero at  $\delta^n$  then slowly increases back to 1. The transmittance reaches its minimum value  $T^n = 0$  when  $n = 9$  while the reflectance reaches its maximum value  $R^n = 1$  at  $\delta^n$ . Further increasing the photon number to  $n = 25$ , frequency-independent perfect transmission is achieved again. However, the conversion probabilities remains zero for any  $\Delta_k^n$  in  $1 + 1$ ,  $9 + 1$  and  $25 + 1$  subspace. These discussions demonstrate that under given parameters with  $\Gamma, \tau$  etc. BICs

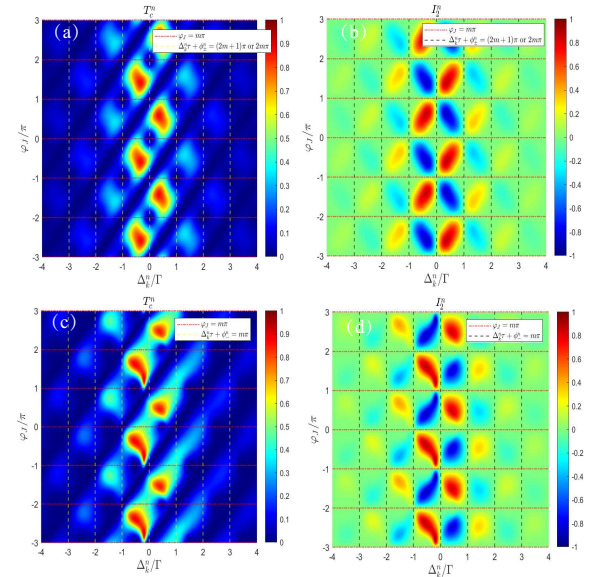


FIG. 6. (a,c) The conversion probability  $T_c^n$  and (b,d) the conversion contrast  $I_2^n$  versus phase  $\varphi_J$  and the scaled detuning  $\Delta_k^n/\Gamma$  for (a,b)  $\phi_+^n = \pi$ , (c,d)  $\phi_+^n = \pi/2$ , when  $|J_1| = |J_2|$ ,  $\omega_{fc} = 0$ ,  $\tau\Gamma = \pi$ ,  $\phi_-^n = 0$ .

can simultaneously emerge in the  $n_-$ -channel of different subspaces, which is evidenced by the perfect transmission observed in both the  $1 + 1$  and the  $25 + 1$  subspaces. Alternatively, BICs can occur in the  $n_-$ -channel of one subspace while appearing in the  $n_+$ -channel of another subspace evidenced by the perfect transmission in the  $1 + 1$  subspace while perfect reflection in the  $9 + 1$  subspace. In addition, BICs can also simultaneously emerge in the  $n_+$ -channel of different subspaces. All of these can be controlled by setting the initial state of the resonator. The vanishing of frequency conversion signifies the emergence of BIC. Thus, preventing the formation of BICs enhances the conversion probability. However, the optimal conversion probability is at most, one-half (see the maximum values in Fig.3 and Fig.4), which originates from the reciprocity of photon transmission. In Fig.5, we plot the influence of the number  $n$  of photons in the resonator on the conversion contrast and the corresponding profiles at some subspaces with parameters  $\omega_e, g, \tau, \Gamma$  presenting reciprocal spectra in the  $1 + 1$  subspace. It can be seen that  $I_2^n = 0$  when  $n = 1$ , the conversion contrast first rises from 0 to a maximum at  $n = 4$ , later on returns to its original value 0 at  $n = 9$ , then gradually drops to a minimum at  $n = 16$ . This demonstrates that altering the photon number in the resonator induces the non-reciprocal transmission of single photons in the waveguide. The maximum and minimum values appear at  $\Delta_k^n = \delta^n$ , and  $I_2^n$  achieves the optimal maximum 1 and the optimal minimum  $-1$  at position  $\Delta_k^n = 0$  when  $\varphi_J = \pi/2$  (see Fig. 5(d)).

## B. Non-Markovian regime

The Markovian approximation can be violated when the coupling between the system and its environment is strong or when there is not a clear separation between the typical timescales associated with the system and the environment, here, we consider the situation with the travel time  $\tau$  of light between coupling points comparable to the characteristic timescale  $\Gamma^{-1}$ . Phase factors are now detuning-dependent. In Fig. 6, we have plotted the conversion probability  $T_c^n$  and the conversion contrast  $I_2^n$  versus phase  $\varphi_J$  and the scaled detuning  $\Delta_k^n/\Gamma$  for  $n = 1$ . When  $\varphi_J = (m + 1/2)\pi$ , different from the Lorentzian lineshape in the Markovian regime, the conversion probability exhibits multiple peaks and dips. When  $\varphi_J = m\pi$ , the conversion probability vanishes only at certain frequencies with  $\Delta_k^n\tau = m\pi$ , see the intersection between the red dotted line and the white dashed line in Fig. 6a. We still can observe that  $T_c^n = 0$  at locations  $\Delta_k^n\tau = 2m\pi$  when  $\varphi_J = (2m + 1)\pi$  in Fig. 6c, however, the locations  $\Delta_k^n\tau = (2m + 1)\pi$  of  $T_c^n = 0$  in Fig. 6a are changed to  $\Delta_k^n\tau = (2m - 1/2)\pi$  in Fig. 6c. For  $\varphi_J = 2m\pi$ ,  $\Delta_k^n\tau = (2m + 1)\pi$  also lead to  $T_c^n = 0$  in Fig. 6c, however, locations  $\Delta_k^n\tau = 2m\pi$  in Fig. 6a are changed to  $\Delta_k^n\tau = (2m + 1/2)\pi$ . The locations  $\Delta_k^n\tau = 2m\pi$  ( $\Delta_k^n\tau = (2m + 1)\pi$ ) of the conversion dips can be regarded as static zeroes for  $\varphi_J = (2m + 1)\pi$  ( $\varphi_J = 2m\pi$ ). These static zeros are related to phase  $\phi_-^n$  since it remains constant in Fig. 6a and 6c, the moving zeros are related to phase  $\phi_+^n$ , which help us to find that the static zeros satisfy  $\Delta_k^n\tau + \phi_-^n = 2m\pi$  for  $\varphi_J = (2m + 1)\pi$  or  $\Delta_k^n\tau + \phi_-^n = (2m + 1)\pi$  for  $\varphi_J = 2m\pi$ , resulting in complete suppression of the emission from the  $|e\rangle \leftrightarrow |n_-\rangle$  transition to the waveguide; the moving zeros satisfy  $\Delta_k^n\tau + \phi_+^n = 2m\pi$  for  $\varphi_J = (2m + 1)\pi$  or  $\Delta_k^n\tau + \phi_+^n = (2m + 1)\pi$  for  $\varphi_J = 2m\pi$ , resulting in complete suppression of the emission from the  $|e\rangle \leftrightarrow |n_+\rangle$  transition to the waveguide. It can be concluded that a zero conversion probability, in both Markovian and non-Markovian regions, serves as a signature for the complete suppression of the emission from the excited state to either of the lower states. In addition, the conversion dips located at  $\Delta_k^n\tau = 2m\pi$  moves toward the blue-shift direction as  $\varphi_J$  increases in both Fig. 6a and Fig. 6c. We also found that the conversion dips occur along the line  $\Delta_k^n\tau + \phi_-^n - \varphi_J = (2m + 1)\pi$  and  $T_c^n \leq 1/2$  along the line  $\varphi_J = m\pi$ . The conversion contrast always vanishes along the line  $\varphi_J = m\pi$  since the system is reciprocal for photons (see the red dotted line in Fig. 6b and 6d), which is same as the conversion contrast in the Markovian regime. However, a significant difference appear for both regimes for  $\varphi_J \neq m\pi$ . It can be seen that the conversion probability is always reciprocal leading to  $I_2^n = 0$  as long as  $\phi_-^n = m\pi$  in the Markovian regime, however,  $I_2^n = 0$  only occurs at certain frequencies Fig. 6(b,d), indicating that the system generally exhibits non-reciprocity. This non-reciprocity is induced by non-Markovian effects. It is easy to find from Fig. 6b and 6d that  $I_2^n = 0$  as long

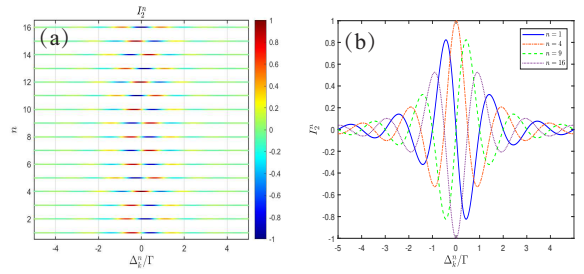


FIG. 7. (a) The conversion contrast  $I_2^n$  versus photon number  $n$  and the scaled detuning  $\Delta_k^n/\Gamma$  when  $|J_1| = |J_2|$ ,  $\omega_{fc} = 0$ ,  $\omega_e/\Gamma = 995.5$ ,  $g/\Gamma = 5.5$ ,  $\tau\Gamma = \pi$ ,  $\varphi_J = 0.5\pi$ . (b) The profile of the conversion contrast at  $n = 1, 4, 9, 16$ .

as  $\Delta_k^n\tau + \phi_-^n = m\pi$ . Since  $I_2^n = -I_1^n$ , the disappearance of contrasts can be understood from the interference of the transmitted wave. For a plane wave incident from the left (right) of the giant atom, there are two paths propagating to the right (left) of the giant atom: in the first path, the wave transmits directly along the waveguide to the position  $x > d/2$  ( $x < -d/2$ ), accumulating a phase of  $\Delta_k^n\tau$ , in the second path, waves propagate through the GA to  $x > d/2$  ( $x < -d/2$ ), accumulating a phase of  $\Delta_k^n\tau + \phi_-^n + \varphi_J$  ( $\Delta_k^n\tau + \phi_-^n - \varphi_J$ ). The waves transmitting directly through the waveguide cancel each other. The difference between these two waves undergoing the second path can be regarded as the superposition of two waves traveling in the same direction, except that there is a phase difference of between them, i.e., one wave accumulates a phase of  $\Delta_k^n\tau + \phi_-^n + \varphi_J$ , the other wave accumulates a phase of  $\pi + \Delta_k^n\tau + \phi_-^n - \varphi_J$ . These two waves interference destructively when  $\Delta_k^n\tau + \phi_-^n = m\pi$  or  $\varphi_J = m\pi$ . Furthermore, we can also observe that in Fig. 6b, for any given phase  $\varphi_J$ ,  $I_2^n$  is symmetric about the point  $\Delta_k^n = 0$ , whereas this is not the case in 6d. For any given detuning  $\Delta_k^n$ , both Fig. 6b and 6d exhibit symmetry about the point  $\varphi_J = 0$ .

To show that the number  $n$  of photons in the resonator can tune the transport properties of photons, we plot the conversion contrast versus the scaling detuning and the photon number  $n$  in the resonator when  $\varphi_J = \pi/2$  in Fig. 7 with given parameters  $\omega_e, g, \tau, \Gamma$ . In the subspace with  $n = 1$ , the maximum value of  $I_2^n$  appears on the left side of  $\Delta_k^n = 0$ , and the curve is symmetric about the point  $\Delta_k^n = 0$  (see the blue solid line in Fig. 7b). As  $n$  increases, the maximum initially shifts to the left, then moves to the right. At  $n = 4$ ,  $I_2^n$  reaches its maximum value of 1, which occurs exactly at  $\Delta_k^n = 0$ , and the curve becomes symmetric about the axis  $\Delta_k^n = 0$  (see the orange dash-dotted line in Fig. 7b). Subsequently, the value of  $I_2^n$  decreases and moves to the right, later oscillating on both sides of the axis  $\Delta_k^n = 0$ . Notably, the profile of  $I_2^n$  at  $n = 9$  is the mirror image of that at  $n = 1$  with respect to the axis  $\Delta_k^n = 0$  (see the green dashed line in Fig. 7b), and at  $n = 12$ , the value of  $I_2^n$  approaches unity meaning  $T_c^n \rightarrow 1$  and  $\tilde{T}_c^n \rightarrow 0$ , and the location of this maximum lies close to  $\Delta_k^n = 0$ . At  $n = 16$ ,

a curve symmetric about the axis  $\Delta_k^n = 0$  reappears, but at this time,  $I_2^n$  attains its minimum value of  $-1$  (see the purple dotted line in Fig.7b) indicating  $T_c^n = 0$  and  $\tilde{T}_c^n = 1$ . One can see that the frequency conversion can be adjusted not only by the accumulated phases but also by the initial state of the resonator.

#### IV. CONCLUSION

We have studied the transport of a single photon propagating in a 1D conventional waveguide. The scattering target is a V-type GA. One of the GA's transition is coupled to a 1D waveguide at two coupling points and the other transition is coupled to a single-mode resonator. The presence of photons in the resonator triggers the frequency conversion of single photons in the 1D waveguide, and the frequency shift is controlled by the number of photons in the resonator. The single-photon scattering spectra are obtained by utilizing a real-space scattering method when the GA and the resonator contain  $n$  excitations. We analyze the influences of phase delay between coupling points, the phase difference  $\varphi_J$  between two GA-waveguide couplings and the number of photons in the resonator on the scattering spectra and the conversion contrast characterizing the non-reciprocity in both the Markovian and the non-Markovian regimes. The spectra of the conversion probability exhibit multiple peaks and dips in the non-Markovian regime instead of the Lorentz

lineshape in the Markovian regime. The zero conversion probability, produced by the quantum interference induced by the scale of a V-type GA characterized by phase delay  $\phi_{\pm}^n$ , serves as a signature for the complete suppression of the emission from the excited state to either of the lower states in both Markovian and non-Markovian regions. The optimal maximum of the conversion probability is at most one-half when the system is reciprocal. In particular, the conversion contrast keep the constant value 0 in the Markovian regime when  $\varphi_J \neq m\pi$  and  $\phi_{\pm}^n = m\pi$ , one can break this reciprocity by either changing the number of the excitations in the GA and the resonator in the Markovian regime to enhance single-photon conversion efficiency to unity, or increasing the distance of the two coupling points so that the delay time is comparable to the lifetime of the GA. In the non-Markovian regime, adjusting the number of the excitations in the GA and the resonator changes the conversion contrast from the minimum to the maximum, which achieves single-photon frequency up- or down-conversion with unity efficiency.

#### ACKNOWLEDGMENTS

This work was supported by NSFC Grants No.12421005, No.12247105, XJ-Lab Key Project (23XJ02001), and the Science & Technology Department of Hunan Provincial Program (2023ZJ1010).

---

[1] H. J. Kimble, The quantum internet, *Nature* (London) 453, 1023 (2008).

[2] C. L. Degen, F. Reinhard and P. Cappellaro, Quantum sensing, *Rev. Mod. Phys.* 89, 035002 (2017).

[3] V. Giovannetti, S. Lloyd, and L. Maccone, Quantum Metrology, *Phys. Rev. Lett.* 96, 010401 (2006).

[4] D. Roy, C. M. Wilson, and O. Firstenberg, Strongly interacting photons in one-dimensional continuum, *Rev. Mod. Phys.* 89, 021001 (2017).

[5] A. S. Sheremet, M. I. Petrov, I. V. Iorsh, A. V. Poshakinskiy, A. N. Poddubny, Waveguide quantum electrodynamics: Collective radiance and photon-photon correlations, *Rev. Mod. Phys.* 95, 015002 (2023).

[6] M. Bradford, K. C. Obi, and J.-T. Shen, Efficient Single-Photon Frequency Conversion Using a Sagnac Interferometer, *Phys. Rev. Lett.* 108, 103902 (2012);

[7] M. Bradford, J.-T. Shen, Single-photon frequency conversion by exploiting quantum interference, *Phys. Rev. A* 85, 043814 (2012).

[8] Z. H. Wang, L. Zhou, Y. Li, and C. P. Sun, Controllable single-photon frequency converter via a one-dimensional waveguide, *Phys. Rev. A* 89, 053813 (2014).

[9] W. Z. Jia, Y. W. Wang, and Y.-X. Liu, Efficient single-photon frequency conversion in the microwave domain using superconducting quantum circuits, *Phys. Rev. A* 96, 053832 (2017).

[10] L. Zhou, Y. Chang, H. Dong, L.-M. Kuang, and C. P. Sun, Inherent Mach-Zehnder interference with "which-way" detection for single particle scattering in one dimension, *Phys. Rev. A* 85, 013806 (2012).

[11] Z. L. Lu, J. Li, J. Lu, and L. Zhou, Controlling atom-photon bound states in a coupled resonator array with a two-level quantum emitter, *Opt. Lett.* 49, 806 (2024).

[12] J. Li, J. Lu, L. Xu, and L. Zhou, Phase Control of Single-Photon States in 1D Coupled-Resonator Waveguide, *Adv. Quantum Technol.* 8, e2500270 (2025).

[13] G. Andersson, B. Suri, L. Guo, T. Aref, and P. Delsing, Non-exponential decay of a giant artificial atom, *Nat. Phys.* 15, 1123 (2019).

[14] S. Longhi, Photonic simulation of giant atom decay, *Opt. Lett.* 45, 3017 (2020).

[15] F. Roccati, and D. Cilluffo, Controlling Markovianity with Chiral Giant Atoms, *Phys. Rev. Lett.* 133, 063603 (2024).

[16] A. C. Santos and R. Bachelard, Generation of Maximally Entangled Long-Lived States with Giant Atoms in a Waveguide, *Phys. Rev. Lett.* 130, 053601 (2023).

[17] A. F. Kockum, G. Johansson, and F. Nori, Decoherence-Free Interaction between Giant Atoms in Waveguide Quantum Electrodynamics, *Phys. Rev. Lett.* 120, 140404 (2018).

[18] A. Soro and A. F. Kockum, Chiral quantum optics with giant atoms, *Phys. Rev. A* 105, 023712 (2022).

[19] W. J. Gu, L. Chen, Z. Yi, S. J. Liu, and G.-X. Li, Tunable photon-photon correlations in waveguide QED systems with giant atoms, *Phys. Rev. A* 109 023720 (2024).

[20] M. Z. Weng, H. W. Yu, and Z. H. Wang, High-fidelity generation of Bell and W states in a giant-atom system via bound states in the continuum, *Phys. Rev. A* 111 053711 (2025).

[21] X.-L. Yin, H.-W. J. Lee, and G. F. Zhang, Giant-atom dephasing dynamics and entanglement generation in a squeezed vacuum reservoir, *Phys. Rev. A* 111 033707 (2025).

[22] L. Du, M. R. Cai, J. H. Wu, Z. H. Wang, and Y. Li, Single photon nonreciprocal excitation transfer with non-Markovian retarded effects, *Phys. Rev. A* 103, 053701 (2021).

[23] H. W. Yu, Z. H. Wang, and J.-H. Wu, Entanglement preparation and nonreciprocal excitation evolution in giant atoms by controllable dissipation and coupling, *Phys. Rev. A* 104, 013720 (2021).

[24] M. V. Gustafsson, T. Aref, A. F. Kockum, M. K. Ekström, G. Johansson, and P. Delsing, Propagating phonons coupled to an artificial atom, *Science* 346, 207 (2014).

[25] R. Manenti, A. F. Kockum, A. Patterson, T. Behrle, J. Rahamim, G. Tancredi, F. Nori, and P. J. Leek, Circuit quantum acoustodynamics with surface acoustic waves, *Nat. Commun.* 8, 975 (2017). (2017).

[26] G. Andersson, M. K. Ekström, and P. Delsing, Electromagnetically Induced Acoustic Transparency with a Superconducting Circuit, *Phys. Rev. Lett.* 124, 240402 (2020).

[27] A. M. Vadiraj, A. Ask, T. G. McConkey, I. Nsanzineza, C. W. Sandbo Chang, A. F. Kockum, and C. M. Wilson, Engineering the level structure of a giant artificial atom in waveguide quantum electrodynamics, *Phys. Rev. A* 103, 023710 (2021).

[28] L. Du and Y. Li, Single-photon frequency conversion via a giant  $\Lambda$ -type atom, *Phys. Rev. A* 104, 023712 (2021).

[29] L. Du, Y.-T. Chen, and Y. Li, Nonreciprocal frequency conversion with chiral  $\Lambda$ -type atoms, *Phys. Rev. Res.* 3, 043226 (2021)

[30] J.-T. Shen and S. Fan, Coherent Single Photon Transport in a One-Dimensional Waveguide Coupled with Superconducting Quantum Bits, *Phys. Rev. Lett.* 95, 213001 (2005).

[31] L. Zhou, Z. R. Gong, Y.-X. Liu, C. P. Sun, and F. Nori, Controllable Scattering of a Single Photon inside a One-Dimensional Resonator Waveguide, *Phys. Rev. Lett.* 101, 100501 (2008).

[32] L. Z. Guo, A. F. Kockum, F. Marquardt, and G. Johansson, Oscillating bound states for a giant atom, *Phys. Rev. Res.* 2, 043014 (2020).

[33] X. Wang, T. Liu, A. F. Kockum, H.-R. Li, and F. Nori, Tunable chiral bound states with giant atoms, *Phys. Rev. Lett.* 126, 043602 (2021).

[34] K. H. Lim, W.-K. Mok, and L.-C. Kwek, Oscillating bound states in non-Markovian photonic lattices, *Phys. Rev. A* 107, 023716 (2023).

[35] X. J. Zhang, C. G. Liu, Z. R. Gong, and Z. H. Wang, Quantum interference and controllable magic cavity QED via a giant atom in a coupled resonator waveguide, *Phys. Rev. A*, 108, 013704 (2023).

[36] Z. Y. Li and H. Z. Shen, Non-Markovian dynamics with a giant atom coupled to a semi-infinite photonic waveguide, *Phys. Rev. A* 109, 023712 (2024).

[37] Y. Y. Yan and Z. G. Lv, Controllable spontaneous emission spectrum in an artificial giant atom: Dark lines and bound states, *Phys. Rev. Res.* 6, 013301 (2024).

[38] D.-W. Wang, C. S. Zhao, Y.-T. Yan, J. Y. Yang, Z. H. Wang, and L. Zhou, Topology-dependent giant-atom interaction in a topological waveguide QED system, *Phys. Rev. A* 109, 053720 (2024).

[39] Y. Yang, G. Sun, J. Li, J. Lu, and L. Zhou, Coherent Control of Spontaneous Emission for a giant driven  $\Lambda$ -type three-level atom, *Phys. Rev. A*, 111, 013707 (2025).

[40] G. Sun, Y. Yang, J. Li, J. Lu, and L. Zhou, Cavity-modified oscillating bound states with a  $\Lambda$ -type giant emitter in a linear waveguide, *Phys. Rev. A*, 111, 033701 (2025).

[41] Y. P. He, G. Sun, J. Li, Y. Yang, J. Lu, and L. Zhou, Emergent Oscillating bound states in a semi-infinite linear waveguide with a point-like  $\Lambda$ -type quantum emitter driven by a classical field, *Adv. Quantum Technol.*, 8, 2400535 (2025)